CCFE
CULHAM CENTRE FOR FUSION ENERGY

UK Atomic Energy Authority

UKAEA-CCFE-PR(18)57

D. Darby-Lewis , J. Tennyson, K. D. Lawson, S. N. Yurchenko, M. F. Stamp, A. Shaw, S. Brezinsek

Synthetic spectra of BeH, BeD and BeT for emission modelling in JET plasmas

Synthetic spectra of BeH, BeD and BeT for emission modelling in JET plasmas

D. Darby-Lewis , J. Tennyson, K. D. Lawson, S. N. Yurchenko, M. F. Stamp, A. Shaw, S. Brezinsek

This is a preprint of a paper submitted for publication in Journal of Physics B

Synthetic spectra of BeH, BeD and BeT for emission modelling in JET plasmas

D. Darby-Lewis[1], J. Tennyson[1], K. D. Lawson[2], S. N. Yurchenko[1], M. F. Stamp[2], A. Shaw[2], S. Brezinsek[3] & JET Contributors[a]

[1]Department of Physics & Astronomy, University College London,Gower St.,London, WC1E 6BT, UK.
[2]CCFE, Culham Science Center, Abingdon, OX14 3DB, UK.
[3]Institut fr Energie und Klimaforschung - Plasmaphysik Forschungszentrum Jülich GmbH Wilhelm-Johnen-Straße, 52428 Jülich, Germany
[a]See the author list of "X. Litaudon et al 2017 Nucl. Fusion **57** 102001"

E-mail: daniel.darby.11@ucl.ac.uk,j.tennyson@ucl.ac.uk, kerry.lawson@ukaea.uk

Abstract. We present a theoretical model for isotopologues of beryllium monohydride, BeH, BeD and BeT, A $^2\Pi$ to X $^2\Sigma^+$ visible and X $^2\Sigma^+$ to X $^2\Sigma^+$ infrared rovibronic spectra. The MARVEL procedure is used to compute empirical rovibronic energy levels for BeH, BeD and BeT, using experimental transition data for the X $^2\Sigma^+$, A $^2\Pi$, and C $^2\Sigma^+$ states. The energy levels from these calculations are then used in the program Duo to produce a potential energy curve for the ground state, X $^2\Sigma$, and to fit an improved potential energy curve (PEC) for the first excited state, A $^2\Pi$, including a spin-orbit (LS) coupling term, a Λ–doubling state to state (A – X states) coupling term, and Born-Oppenheimer breakdown (BOB) terms for both curves. These, along with a previously computed *ab initio* dipole curve for the X and A states are used to generate vibrational-rotational wavefunctions, transition energies and A-values. From the transition energies and Einstein coefficients, accurate assigned synthetic spectra for BeH and its isotopologues are obtained at given rotational and vibrational temperatures. The BeH spectrum is compared with a high resolution hollow-cathode lamp spectrum and the BeD spectrum with high resolution spectra from JET giving effective vibrational and rotational temperatures. Full A – X and X – X linelists are given for BeH, BeD and BeT and also provided on the ExoMol website.

1. Introduction

In order to predict the erosion of the Be first wall in fusion devices such as JET, and in the future ITER, and in view of impurity production and lifetime of components, an understanding of the release and transport of Be is an essential requirement. BeD_X release was shown to contribute more than 50% to the total erosion in certain cases in JET D plasmas in a limiter configuration deduced from BeD emission spectra (Brezinsek et al. 2014).Detailed studies of molecular spectra (Duxbury et al. 1998), such as those for BeH, BeD, and BeT A – X bands can provide valuable input to codes used for erosion modelling, ERO (Borodin et al. 2011), (Lasa et al. 2017). To this end, we have developed a full spectroscopic model for BeH, BeD and BeT X and A states based on explicit potential energy curves (PECs), spin-orbit (LS) and Λ doubling (L^+) couplings, Born-Oppenheimer breakdown (BOB) terms, and *ab initio* dipole curves. The PECs, couplings, and BOB terms are derived using accurate experimentally recorded transition frequencies. Previous PEC fittings for the X state by Le Roy et al. (2006) and Koput (2011) have been improved upon by Dattani (2015), and further refined in this work by fitting procedures involving the X-A state transitions. The A state PEC was previously studied by Le Roy et al. (2006) and is here improved upon. The fitting in Duo (Yurchenko et al. 2018) results in a full set of accurate transitions for BeH, BeD, and BeT from a single set of PECs, couplings, and BOB terms. These data are used to determine temperatures in the experimental spectra.

We present an improved linelist for BeH, BeD and BeT, over the linelist of Yadin et al. (2012) both in having greater scope and improved accuracy in the assigned energies. The present paper aims to give a better fit to the spectrum of the BeD A – X transition than was achieved by Duxbury et al. (1998) and (Björkas et al. 2013) by using more accurate transition data and allowing separation of vibrational and rotational temperatures. The use of different rotational and vibrational temperatures, which implies a non–local thermodynamic equilibrium (non–LTE), is expected to lead to a more accurate description of the experimental spectrum.

We compare theoretically produced synthesized spectra to new experimental BeD spectra recorded on JET and BeH spectra recorded in Be hollow cathode discharges in Forschungszentrum Jülich. Both of these spectra were recorded employing spectrometers with high spectral resolution in the visible range sufficient to resolve the rotational lines.

2. Theory

There are four main steps in generating assigned synthetic spectra fitted with rotational and vibrational temperatures. Experimental transitions are separated into vibronic energy levels using the online implementation of MARVEL (measured active rotation vibration energy levels). These are then used in Duo to fit PECs which can reproduce all the provided energy levels accurately. Electronic states X $^2\Sigma^+$, A $^2\Pi$ and C $^2\Sigma^+$ are present in the MARVEL empirical energy levels, although PECs were fitted only for the

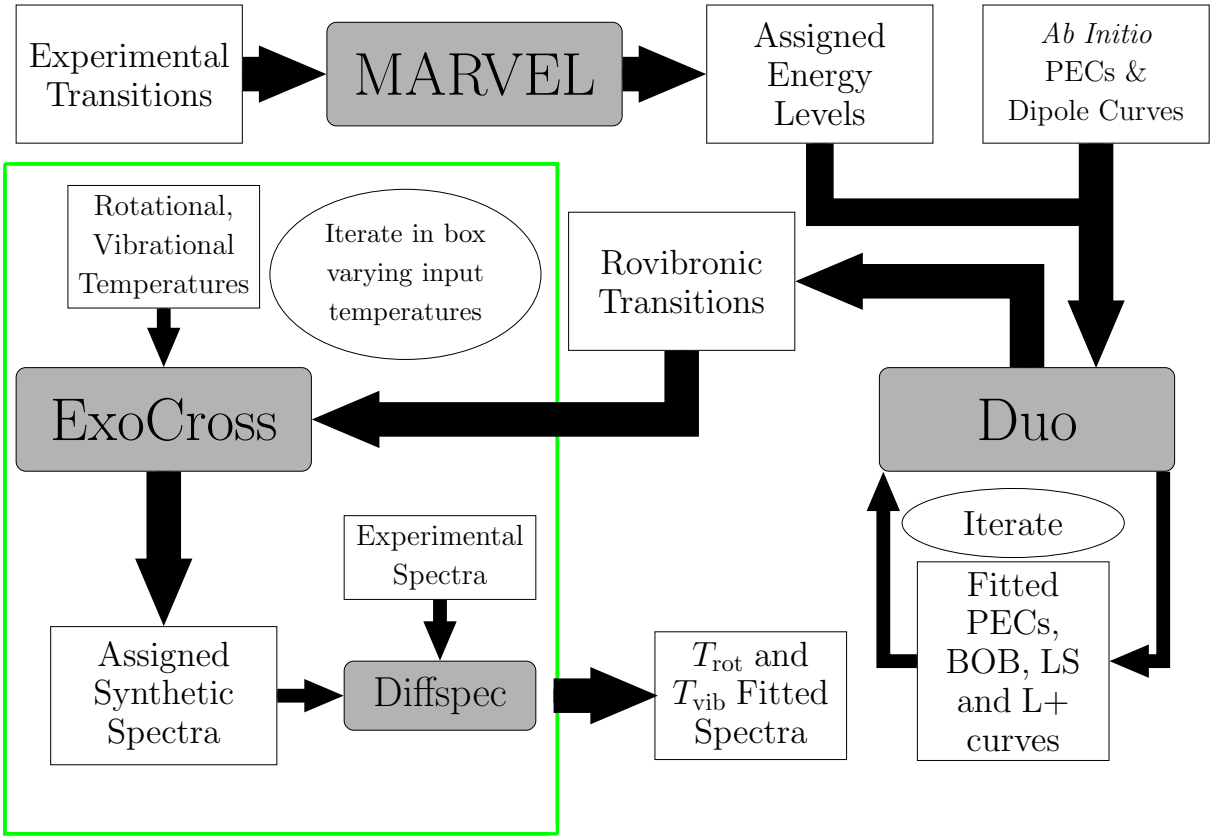

Figure 1. A flow diagram showing the production of high accuracy synthetic spectra, starting in the top left corner with collated experimental transitions and resulting in, bottom centre, synthetic spectra with the best fit rotational and vibrational temperatures.

X and A states. This is because of a lack of transition data for the C state, which in any case does not give rise to a significant feature in the JET emission spectrum. To date, the molecular spectrum is dominated by the A – X band. Consequently, Duo uses an X to A transition dipole to produce values for the observed X to A transitions. The output from Duo contains all transitions between states within a given wavenumber range (parameter in the Duo input, see supplementary data) and all the Einstein coefficients (A-values) associated with those energy levels. These are used by ExoCross to generate synthetic spectra with varying rotational and vibrational temperatures. These spectra are compared to experimental spectra to obtain a metric for the fit.The flowchart in Figure 1 illustrates the links between the steps of this process, each step is presented in detail below.

Table 1. Input transitions for MARVEL Online. See text for discussion on the comments

Isotope	Tag	Range (cm^{-1})	States	Transitions	Largest Network	Comments
BeH						
	Le Roy et al. (2006).	15132-20822	A – X, C – X	1887	1264	H1
	Shayesteh et al. (2003).	1802-2239	X – X	160		H2
BeD						
	Le Roy et al. (2006).	15164-20619	A – X, C – X	2276	1495	D1
	Shayesteh et al. (2003).	1240-1680	X – X	167		D2
BeT						
	Le Roy et al. (2006).	19824-20424	A – X, $\Delta v = 0$ only.	524	215	T1

2.1. MARVEL

MARVEL (Furtenbacher et al. 2007, Furtenbacher & Császár 2012) is a program with an online user interface which takes highly accurate experimental transition energies and calculates spectroscopic networks of energy levels. For BeH, BeD and BeT we used transitions involving X $^2\Sigma^+$, A $^2\Pi$ and C $^2\Sigma^+$, with assigned quantum numbers taken from the literature (Le Roy et al. 2006, Shayesteh et al. 2003). In particular Le Roy et al. (2006) give transition data compiled from many sources including Shayesteh et al. (2003), Colin et al. (1983), Focsa et al. (1998) and De Greef & Colin (1974).

Table 1 shows the transition data sources used for input to MARVEL. Comments on individual sources are as follows:

H1 Le Roy et al. (2006) contains A – X transitions $\Delta v = 0$ up to $v'' = 6$, $\Delta v = +1$ up to $v'' = 6$ and some transitions for C – X with $v'' = 0 - 2$ and $v' = 6 - 10$.

H2 Shayesteh et al. (2003) infrared, rovibrational transitions, were duplicated for $\Sigma = \pm 0.5$ giving 314 valid transitions.

D1 Le Roy et al. (2006) contains A – X transitions $\Delta v = 0$ up to $v'' = 6$, $\Delta v = +1$ up to $v'' = 5$ and some transitions for C – X with $v'' = 0$ and $v' = 8 - 12$.

D2 Shayesteh et al. (2003) infrared, rovibrational transitions, were duplicated for $\Sigma = \pm 0.5$ giving 328 valid transitions.

T1 Le Roy et al. (2006) contains only A – X transitions $\Delta v = 0$.

A small portion of the MARVEL input file for BeH is shown in Table 2 where the column format is explained. The number of quantum numbers used for assignment here is 5. The thresholds for changing uncertainties and for deletion were both set to 3. The full files are given in the supplementary data.

These transitions are run through the program and various unlinked spectroscopic networks of energy levels are generated. Separate networks can be joined with "linking" transitions, e.g. joining the degenerate spin up and spin down states of the ground state with a "transition" of zero energy from one degenerate state to another. The result of this process is to give a large set of accurate energy levels with quantum number assignments. For BeH and BeD the infrared data of Shayesteh et al. (2003) brings together separate vibrational networks. This results in two large networks

Table 2. Table of MARVEL input transitions for BeH with column labels and explanations.

1	2	3	4	5	6	7	8	9	10	11	12	13
$\tilde{v}$	$\Delta\tilde{v}$	State$'$	v'	$(J'+\frac{1}{2})$	P'	Σ'	State$''$	v'	$(J''+\frac{1}{2})$	P''	Σ''	ID
20.3282	0.001	1	0	1	-	-0.5	1	0	1	+	0.5	MAGIC.001
15132.42	0.1	3	0	13	+	0.5	1	9	14	-	0.5	LeRoy.00001
15204.53	0.1	3	0	12	-	0.5	1	9	13	+	0.5	LeRoy.00002
15224.66	0.1	3	0	22	-	0.5	1	8	23	+	0.5	LeRoy.00003
15273.77	0.2	3	0	11	+	0.5	1	9	12	-	0.5	LeRoy.00004
15335.3	0.1	3	0	21	+	0.5	1	8	22	-	0.5	LeRoy.00005
15339.62	0.1	3	0	10	-	0.5	1	9	11	+	0.5	LeRoy.00006
15401.44	0.1	3	0	9	+	0.5	1	9	10	-	0.5	LeRoy.00007
15433.71	0.1	3	0	13	+	0.5	1	9	12	-	0.5	LeRoy.00008
15458.91	0.1	3	0	8	-	0.5	1	9	9	+	0.5	LeRoy.00009
15485.93	0.1	3	0	12	-	0.5	1	9	11	+	0.5	LeRoy.00010

Column	Notation	
1	$\tilde{v}$	Transition frequency (cm^{-1}).
2	$\Delta\tilde{v}$	Estimated uncertainty in transition frequency (cm^{-1}).
3	State$'$	Initial electronic state, 1 = X $^2\Sigma^+$, 2 = A $^2\Pi$, 3 = C $^2\Sigma^+$.
4	v'	Initial vibrational quantum number
5	$(J'+\frac{1}{2})$	Initial total angular momentum quantum number plus 0.5.
6	P'	Initial parity quantum number
7	Σ'	Initial electron angular momentum quantum number
8	State$''$	Final electronic state, 1 = X $^2\Sigma^+$, 2 = A $^2\Pi$, 3 = C $^2\Sigma^+$.
9	v''	Final vibrational quantum number
10	$(J''+\frac{1}{2})$	Final total angular momentum quantum number plus 0.5.
11	P''	Final parity quantum number
12	Σ''	Final electron angular momentum quantum number
13	ID	Unique ID for transition with source label and counting number.

separated along the quantum number Σ, where Σ = -0.5 for one network and Σ = 0.5 for the other. These two networks are joined with a linking transition with a magic wavenumber, between states with opposing spin, as shown for BeH by the transition labelled MAGIC.001 in Table 2. The value of the magic transition is calculated to produce degeneracy between the states with differing spin at low J.

The "good" quantum numbers in this application are the total rotational quantum number (J) and total parity (+ or -). Quantum numbers of operators not strictly conserved in this application can still be used in state assignment. They are electronic state (X $^2\Sigma^+$, A $^2\Pi$ or C $^2\Sigma^+$), vibrational quantum number (v), nuclear rotational angular momentum (N), projection of total spin angular momentum (Σ), projection of total orbital angular momentum (Λ), and the projection of total electronic angular momentum $\Omega = \Lambda + \Sigma$. This places our representation in Hund's case B (Huber &

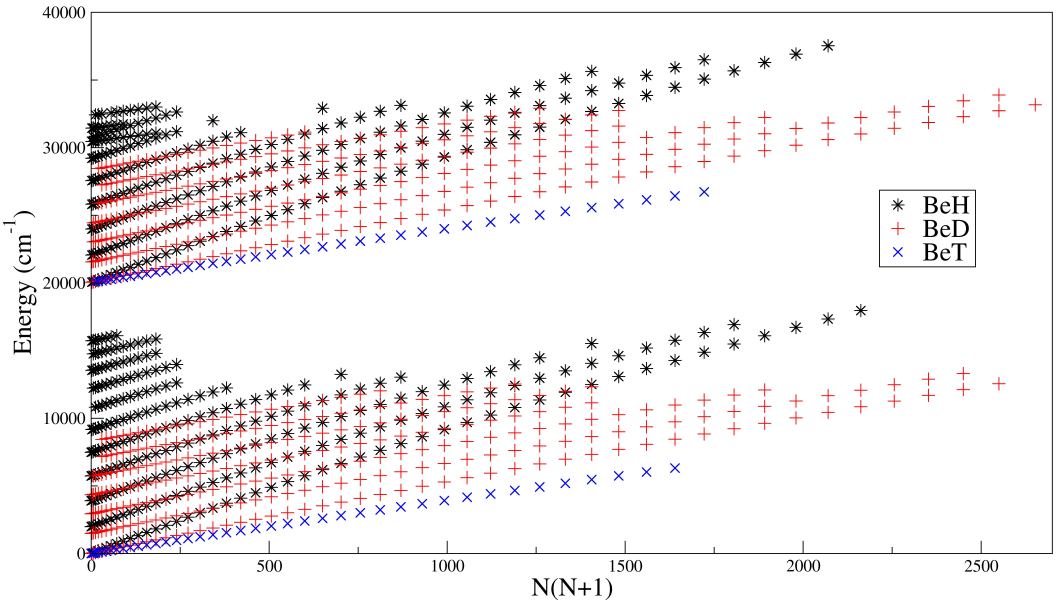

Figure 2. Output rovibronic energy levels from MARVEL for the largest spectroscopic networks of BeH, in black, BeD, in red, and BeT, in blue, against nuclear rotational quantum number, N, times nuclear rotational quantum number plus one. The rovibrational states of X $^2\Sigma^+$ are the lower set and the A $^2\Pi$ rovibrational states start at 20000 cm^{-1}. Each of the states represented here actually corresponds to two spin degenerate states as both the X and the A states are doublets.

Herzberg 1979). Figure 2 shows the rovibrational energy levels of the largest component network for BeH, BeD and BeT. The almost straight lines with isotope dependent gradients, rotational constants ($\propto$ 1/reduced mass), are vibrational bands. Since the electronic states being represented here are doublets each point for an energy level shown in this figure actually corresponds to two spin degenerate states.

2.2. Duo

Duo (Yurchenko et al. 2016) is a nuclear motion code which generates rovibronic wavefunctions for diatomic molecules from PECs, correlation and correction terms. This program contains an iterative fitting procedure where PECs and other terms can be fitted to experimental data. In this way the potential form of the ground state PEC, a Morse long range (MLR) type potential (Le Roy et al. 2011) as given by Pitarch-Ruiz et al. (2008), is refitted using energy levels output from MARVEL. A new PEC, of the extended Morse oscillator (EMO) type, is fitted to the A $^2\Pi$ excited state using energy levels from output from MARVEL. The A $^2\Pi$ PEC is modified by the addition of a spin-orbit (LS) coupling curve and an X to A state L$^+$ (Λ–doubling) coupling curve. Both the ground and excited state PECs are modified by the fitting of adiabatic and non–adiabatic Born–Oppenheimer breakdown (BOB) curves using the BeD and BeT

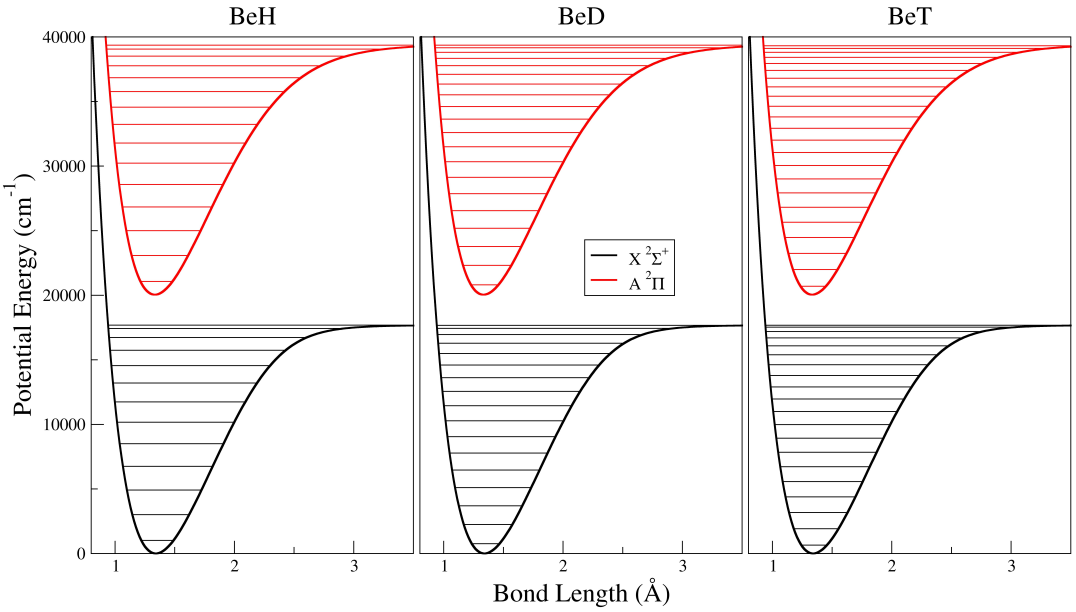

Figure 3. Fitted PECs for the X $^2\Sigma^+$ state and the A $^2\Pi$ state with vibrational energies at $J = 0.5$ for BeH, BeD, and BeT.

isotopologue energy level data from MARVEL. Using BOB correction terms makes these data applicable to all isotopologues of BeH. This allows data from all three isotopologues to improve the fit from the same set of PECs and coupling terms. When a suitable fit is produced for both states using the available energy levels from MARVEL's output Duo allows fittings to be performed using the transitions. This allows a larger set of data to be used in the fitting routine, as some of the energy levels output by MARVEL cannot be connected to the main spectroscopic network.

Tables 3 and 4 show some of the energy levels generated by Duo for BeH, BeD and BeT for both the X and A states, they are each followed by the energies from MARVEL used in the fitting for those levels. As shown earlier in section 2, only the $v = 0$ component of BeT joins the main network of transitions. Overall the root mean square (RMS) of the fit for each isotopologue is: BeH, 0.542477 cm^{-1}; BeD, 0.614474 cm^{-1}; BeT, 0.384016 cm^{-1}. PECs modified and fit by Duo for the X and A states of BeH, BeD and BeT are shown in figure 3. The Zero Point Energy (ZPE) of these fittings are: 1022.0292 cm^{-1} for BeH; 742.7911 cm^{-1} for BeD; 626.2844 cm^{-1} for BeT. The Duo input containing the PECs, couplings and BOB terms is given for BeH, BeD and BeT in the supplementary data. Predissociation is not included in this model.

Fully fitted PECs, couplings and BOB terms are used in conjunction with an *ab initio* transition dipole curve (Pitarch-Ruiz et al. 2008) for the A to X state to generate Einstein A-coefficients for the rovibronic transitions. Duo outputs two files for the linelist of each isotopologue, one containing the list of the states involved in the transitions and the other being a list of the transitions between states and their A-values (Tennyson

Table 3. Comparison of excitation energies as a function of vibrational quanta, v, computed with Duo and obtained by MARVEL for: BeH and BeD X $^2\Sigma^+$ at J=0.5, Ω = 0.5, parity = +; BeT X $^2\Sigma^+$ at J=2.5, Ω = 0.5, parity = -.

v	X $^2\Sigma$					
	BeH		BeD		BeT	
	Duo	MARVEL	Duo	MARVEL	Duo	MARVEL
0	0	0	0	0	49.2756	50.3
1	1986.3054	1986.4169	1488.4401	1488.8472	1323.9046	
2	3896.8004	3896.8707	2935.6045	2936.1953	2568.5846	
3	5729.2711	5729.2613	4340.7423	4341.3802	3782.8768	
4	7480.4545	7480.4219	5702.8860		4966.2478	
5	9145.4221		7020.7372		6118.0189	
6	10716.6777		8292.5346		7237.3131	
7	12182.7098		9515.8791		8322.9914	
8	13525.5493		10687.4899		9373.5704	
9	14716.2767		11802.8549		10387.1133	
10	15705.6510		12855.7188		11361.0802	
11	16402.4285		13837.299		12292.1239	
12	16664.9980		14735.0110		13175.8010	
13			15530.2285		14006.1479	
14			16194.0499		14775.0274	
15			16679.3277		15471.0599	
16			16918.4202		16077.7733	
17			16956.8145		16570.2919	
18					16910.3608	
19					17056.2519	
20					17076.5405	

et al. 2013). The start of the states file and the start of the trans file for BeH are shown respectively in Tables 5 and 6 followed by an explanation of their column formats. The entirety of the linelist states and trans files for each isotopologue can be found in the supplementary data and on the ExoMol website (www.exomol.com).

3. Experiment

3.1. BeH Hollow Cathode Discharge Spectrum

Experimental BeH spectra were recorded using a high resolution visible spectrometer, in cross-dispersion arrangement (grating and prism) covering the spectral range between 373 nm and 680 nm simultaneously in more than 50 orders with an almost constant resolving power of l/DL $\approx$ 20000. The spectral source was a beryllium hollow-cathode

Table 4. Comparison of excitation energies as a function of vibrational quanta, v, computed with Duo and obtained by MARVEL for: BeH and BeD A $^2\Pi^+$ at J=1.5, Ω = 0.5, parity = +; BeT A Π^+ at J=2.5, Ω = 0.5, parity = -.

v	A $^2\Pi$					
	BeH		BeD		BeT	
	Duo	MARVEL	Duo	MARVEL	Duo	MARVEL
0	20050.8587	20092.2658	20048.3803	20071.3872	20089.3230	20090.7
1	22056.7376	22097.0590	21552.7700	21575.8314	21378.1542	
2	23978.5785	24017.3355	23011.6534	23034.2030	22634.0613	
3	25813.4908	25850.6970	24423.8044	24445.6549	23856.2579	
4	27558.2734	27594.5151	25788.0151		25043.9940	
5	29208.9935	29243.2969	27102.9758		26196.4966	
6	30760.6586	30793.4022	28367.1779		27312.9196	
7	32206.9278		29578.8347		28392.3027	
8	33539.8057		30735.8129		29433.5357	
9	34749.2511		31835.5682		30435.3273	
10	35822.6125		32875.0780		31396.1765	
11	36743.7529		33850.7620		32314.3426	
12	37491.6119		34758.3833		33187.8099	
13	38037.6829		35592.9147		34014.2541	
14	38341.2611		36348.3556		34790.9884	
15			37017.4704		35514.9038	
16			37591.4032		36182.3870	
17			38059.0891		36789.2084	
18			38406.3136		37330.3688	
19			38614.1568		37799.8866	
20					38190.4670	
21					38493.0018	
22					38695.7499	
23					38779.4876	

Heraeus discharge lamp with a neon/hydrogen mixture as a working gas. Inside the lamp, the metallic Be target plate is biased, resulting in it being bombarded by the impurity ions with Be being sputtered, either as Be or BeH_X. The current and voltage can be varied changing the plasma characteristics as well as the impact energy of the impinging ions. The released Be or BeH is then excited by electron impact leading to the emission of BeI, BeII as well as BeH light. Figure 4 shows the experimental spectra of the BeH A – X transition as well as the best-fitting simulated spectrum.

Table 5. Section of the states file produced by Duo for BeH with column format explanation.

1	2	3	4	5	6	7	8	9	10	11
n	E	m	J	$P_{+/-}$	$P_{e/f}$	State	v	Λ	Σ	Ω
1	0	16	0.5	+	e	X2Sigma+	0	0	0.5	0.5
2	1986.305446	16	0.5	+	e	X2Sigma+	1	0	0.5	0.5
3	3896.800417	16	0.5	+	e	X2Sigma+	2	0	0.5	0.5
4	5729.271094	16	0.5	+	e	X2Sigma+	3	0	0.5	0.5
5	7480.45445	16	0.5	+	e	X2Sigma+	4	0	0.5	0.5
6	9145.422113	16	0.5	+	e	X2Sigma+	5	0	0.5	0.5
7	10716.677675	16	0.5	+	e	X2Sigma+	6	0	0.5	0.5
8	12182.709789	16	0.5	+	e	X2Sigma+	7	0	0.5	0.5
9	13525.549349	16	0.5	+	e	X2Sigma+	8	0	0.5	0.5
10	14716.276652	16	0.5	+	e	X2Sigma+	9	0	0.5	0.5

Column	Notation	
1	n	Rovibronic counting number.
2	E	Energy of rovibronic state relative to ground state (cm^{-1}).
3	m	multiplicity, including nuclear spin degeneracy.
4	J	Total angular momentum quantum number.
5	$P_{+/-}$	Parity in +/- notation.
6	$P_{e/f}$	Parity in e/f notation.
7	State	Electronic state.
8	v	Vibrational quantum number.
9	Λ	Projection of electronic orbital angular momentum quantum number.
10	Σ	Projection of electron spin angular momentum quantum number.
11	Ω	Projection of total electronic angular momentum quantum number

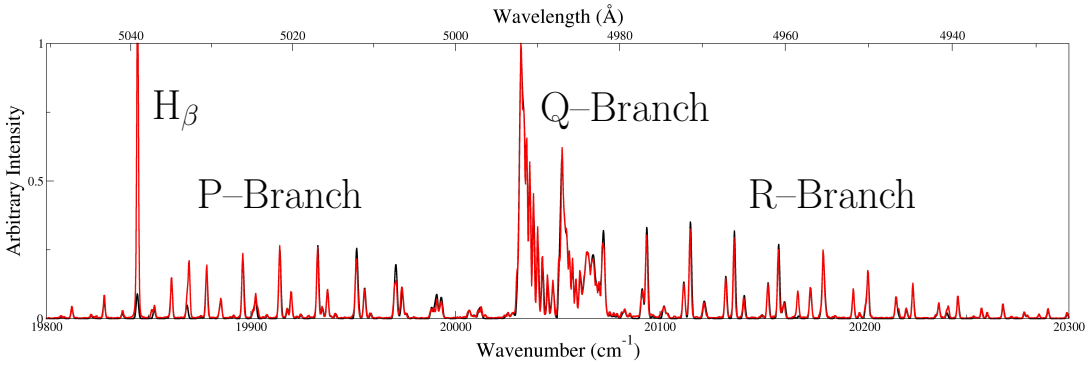

Figure 4. Measured BeH spectrum, shown in red, was recorded with a high resolution visible spectrometer from a hydrogen doped lamp with a beryllium target. Assigned synthetic spectrum of BeH, in black, is generated at $T_{\mathrm{rot}} = 540$ K and $T_{\mathrm{vib}} = 3440$ K from PECs, coupling terms and BOB effects.

Table 6. Section of the trans file produced by Duo for BeH with column format explanation.

1	2	3	4
n''	n'	A	$\tilde{\nu}$
71	1	4.58E-10	16933.174781
89	1	5.63E-02	38037.68383
65	1	8.17E-11	16699.528089
58	1	2.58E-07	12198.141744
95	1	6.48E-03	38492.659618
83	1	1.95E-01	32206.945906
51	1	1.12E-09	20.326390

Column	Notation	
1	n'	Initial rovibronic state number, see table 5
2	n''	Final rovibronic state number, see table 5
3	A	Eisenstein A-coefficient (s^{-1}).
4	$\tilde{\nu}$	Transition wavenumber (cm^{-1}).

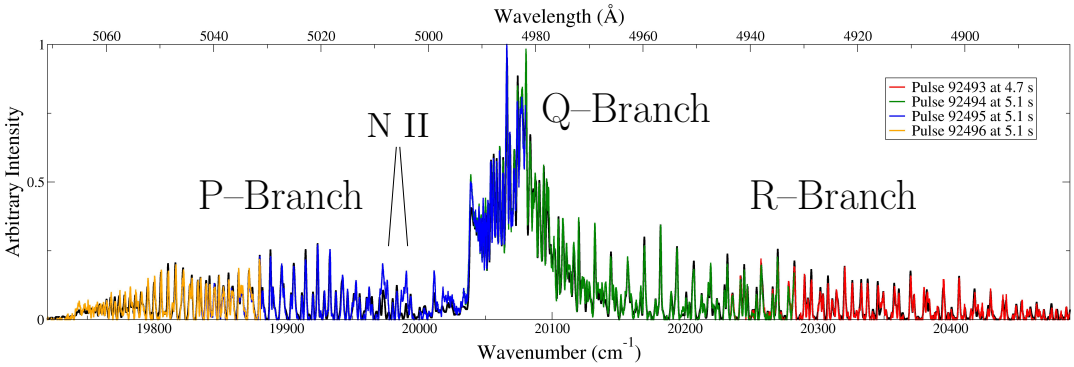

Figure 5. Measured BeD spectra, in red, green, blue and orange lines with pulse numbers and times in the legend, were recorded with a high resolution spectrometer, $T_e \approx 30$ eV and $n_e \approx 10^{-18}$ m^{-3}. Assigned synthetic spectrum, in black, is generated at $T_{rot} = 3800$ K and $T_{vib} = 4700$ K from PECs, coupling terms and BOB effects.

3.2. BeD JET edge emission spectra

An experimental BeD A – X spectrum was measured in four consecutive JET 2.4 T, 2.0 MA discharges with comparable conditions during the limiter phase of the pulse at 4.7 – 5.1 s. During this time, the plasma was limited by the inner poloidal limiter and BeD radiation was emitted from this region. It was recorded with a high resolution visible spectrometer (KS3), which had a Czerny-Turner arrangement and directly observed the low density edge plasma close to the inner poloidal limiter. The spectral wavelength range of the spectrometer does not cover the whole spectrum and so four consecutive discharges were chosen to form a joined image, see figure 5, with comparable plasma conditions as well as assumed comparable rovibrational populations.

4. Spectral Analysis

The final step in generating an assigned synthetic spectra is performed using a program called ExoCross (Yurchenko et al. 2018). ExoCross produces cross-sections for the absorption or emission of photons by molecules. It uses rotational, vibrational and electronic temperatures to produce a statistical (Boltzmann) population model. The equation for the population of a state: $P_{e,v,J}$ where e = electronic state, v = vibrational quanta, and J = total angular momentum quantum number is

$$P_{e,v,J} = e^{-\frac{(E_{e,v,J}-E_{e,v,J=0})}{kT_{\rm rot}}}\ e^{-\frac{(E_{e,v,J=0}-E_{e,v=0,J=0})}{kT_{\rm vib}}}\ e^{-\frac{E_{e,v=0,J=0}}{kT_{\rm ele}}} \quad (1)$$

in which the temperature dependence is split into three exponentials with exponents relating to the rotational, vibrational and electronic state temperatures respectively. The first term is a function of the rotational temperature, $T_{\rm rot}$, and pure rotational energy, $(E_{e,v,J} - E_{e,v,J=0})$, the second the vibrational temperature, $T_{\rm vib}$, and pure vibrational energy, $(E_{e,v,J=0} - E_{e,v=0,J=0})$, and the third the electronic state temperature, $T_{\rm ele}$, and the pure electronic state energy, $E_{e,v=0,=0}$.

Einstein A-values, here provided by Duo, along with the populations are used to generate transition intensities, $I_{e'',v'','e',v','}$. ExoCross then uses line positions, also from Duo, and generates Gaussians with a width of the spectrometer's instrument function, $w \approx 1.5$ Å (≈ 0.6 cm^{-1}), and an area of the calculated transition intensity, $I_{e'',v'','e',v','}$. These individual Gaussians are summed, giving the emitted intensity at a given energy.

In taking different rotational, vibrational and electronic temperatures ExoCross allows us to more accurately fit non–LTE spectra. This procedure is useful in the case where LTE has not been reached by the molecule producing the spectra. In such an instance the different spacing between electronic, vibrational, and rotational energy levels means that they adapt to changing temperatures and plasma conditions at different rates. In the cases discussed here the necessary time to reach equilibrium is too long and the plasma density too low for LTE conditions.

The ExoCross calculation is repeated for rotational and vibrational temperatures varying independently from 500 K to 10000 K. For each combination of vibrational and rotational temperatures a program 'diffspec' is used to integrate the area under both curves, the overlap, and the area between the curves, the difference. The theoretical and experimental spectra are both normalized, in the first instance, to have Q-branch peak values of 1.0. A multiplicative factor is then required to allow the peak values to differ. The experimental spectrum also contains a background which must be removed before matching to the theoretical spectrum, which necessitates a threshold. Also a higher weighting should be placed on fitting to the more intense parts of the experimental spectra which have the smallest experimental uncertainties in measurement. To this end, there are three inputs which adjust the intensity to control the nature of the fitting: factors, background thresholds and weight. The factors are applied to the synthetic spectrum by multiplying the intensity by a series of factors, here 0.8 to 1.2 in steps of 0.05. This allows the normalized spectra of arbitrary intensities to have different

maximum values with respect to one another. For each factor thresholds are applied to the experimental spectra, moving each one up or down by an amount which varies from 0.0 to 0.1 in steps of 0.01. This allows the background in the experimental spectra to be accounted for even if they differ in the spectra recorded in different discharges. The last control input is a weight, allowing a higher weighting to be given to the higher intensity portions of the spectra for both the difference and the overlap. This is achieved by weighting each intensity by a power, here a weighting of 2.0 is used, the area effectively being squared. This ensures a sensible relation between the uncertainty in an intensity measurement and the magnitude of that intensity. There are also input parameters which are set to ignore certain, polluted, regions of the spectra from the area summation.

4.1. BeH Analysis

In Figure 4 and 6 the experimental spectra for BeH is compared with the theoretical spectra generated by the computational methods described in section 2. An invasive H-atom line, H_β, is marked in Figure 4; this region was excluded from the temperature fitting procedure in diffspec as described above. The best fit temperature for this spectra has $T_{\rm rot}$ = 540 K and $T_{\rm vib}$ = 3440 K meaning that the emission is from a non–LTE plasma. The extreme difference between the vibrational and rotational temperatures is a product of the method by which the spectrum was produced. The need for a much higher vibrational temperature is seen if a synthetic spectra for $T_{\rm vib} = T_{\rm rot}$ = 540 K is produced. This would be the spectrum of BeH in LTE at 540 K and it clearly shows all of the primary peaks, that is all the transitions from fundamental vibrational quanta $v' = 0$ to $v'' = 0$. What is missing are all the lower intensity peaks which are produced by transitions from higher vibrational states. When the vibrational temperature is brought up to the best fit temperature of 3440 K the lower intensity, higher vibrational, components of the spectrum are brought sharply into alignment with the experimentally observed spectrum.

The degree of matching to the experimental spectra is highlighted by the close–up view of the R-branch shown in Figure 6. The transition assignment labels here show how the vibrational quanta $v' = 0$ – $v'' = 0$ transitions are more intense and those of higher vibrational quanta are lower in intensity. The assignments show in order left to right: v' = upper state vibrational quantum number, N' = upper state nuclear rotational quantum number, v'' = lower state vibrational quantum number, N'' = lower state nuclear rotational quantum number. The heights of the transition lines in this figure are proportional to the A-values of the transitions not to the transition intensities. Hence, these lines do not necessarily correspond one to one to the height of the peaks in the synthetic spectrum which are dependent on temperature based populations, see Eq (1), as well as A-values.

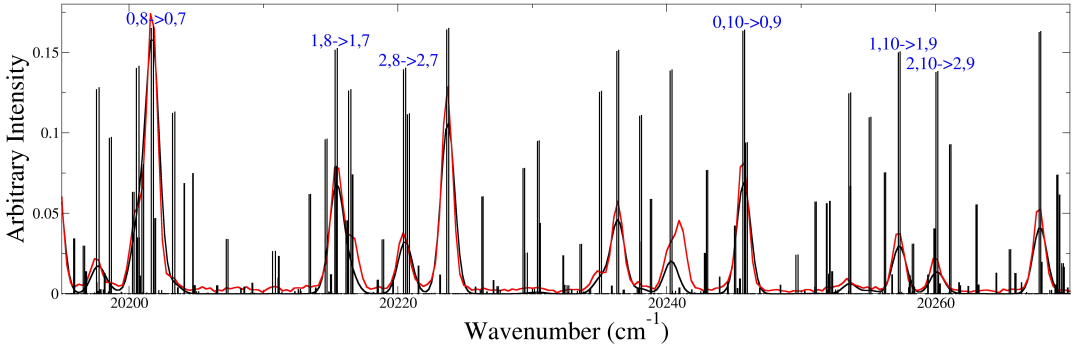

Figure 6. Magnified R-branch synthetic BeH A – X spectrum as in Figure 4, generated at $T_{\rm rot}$ = 540 K and $T_{\rm vib}$ = 3440 K. Measured BeH spectrum is shown in red and transition assignments with drop lines in black. Assignments show the upper state vibrational quantum number, upper state nuclear rotational quantum number –> upper state vibrational quantum number, upper state nuclear rotational quantum number.

4.2. BeD Analysis

A match was made between the experimental BeD spectrum from JET and a theoretical spectrum by varying the vibrational and rotational temperatures. Figure 5 shows an assigned synthetic spectrum generated at $T_{\rm rot} = (3800 \pm 200)$ K and $T_{\rm vib} = (4700 \pm 100)$ K from PECs, coupling terms and BOB effects. Measured BeD spectra were recorded during the limiter phase of discharges 92493 - 92496. The vibrational and rotational temperatures fitted to the joined spectrum for BeD are much closer than in the BeH spectrum above, meaning the plasma conditions were much closer to LTE. There are four features, around ≈ 20000 cm^{-1} in the JET spectra which are not reproduced in the synthetic spectrum. These are invasive features from other species, two being impurity lines of remaining nitrogen in the plasma.

Figure 7 shows a close up section of the Q–branch with black drop lines at every transition energy in the region. This figure demonstrates the high degree of accuracy present across the range of these calculations.

The paper by Duxbury et al. (1998) shows fittings for several molecular features in JET spectra including a BeD spectrum of the A to X transition. They fit a synthetic spectrum to an observed spectrum, which is generated using molecular constants. These are only valid for each isotope individually. By visual comparison, our work shows an improvement in line positions and in intensities.

4.3. BeT Predictions

Figure 8 shows a predicted synthetic spectrum of the A – X transition of BeT. The rotational and vibrational temperatures used to generate this spectrum are those found for BeD in the JET discharges discussed before. This is the BeT rovibronic spectrum

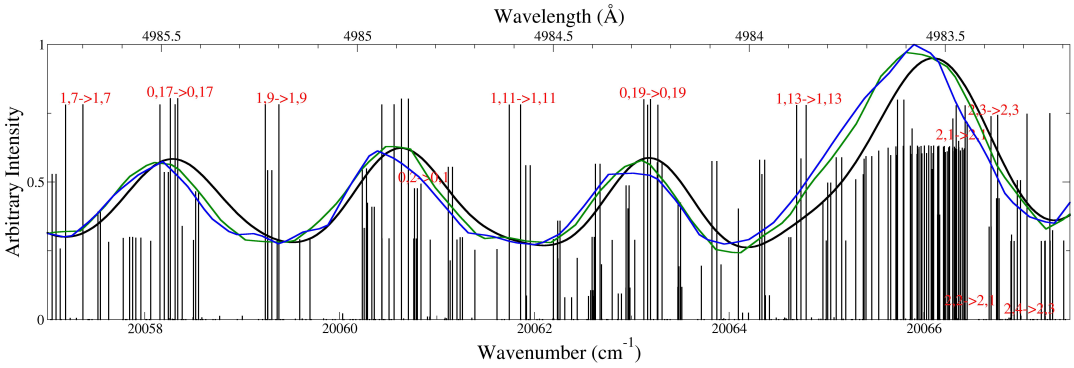

Figure 7. Magnified Q-Branch synthetic BeD A – X spectra as in Figure 5, generated at $T_{\rm rot}$ = 3800 K and $T_{\rm vib}$ = 4700 K . Transition assignments with drop lines in black and high resolution JET measured spectra in green and blue. Assignments show in order left to right: v'' = upper vibrational quantum number, N'' = upper nuclear rotational quantum number, v' = lower vibrational quantum number, N' = lower nuclear rotational quantum number.

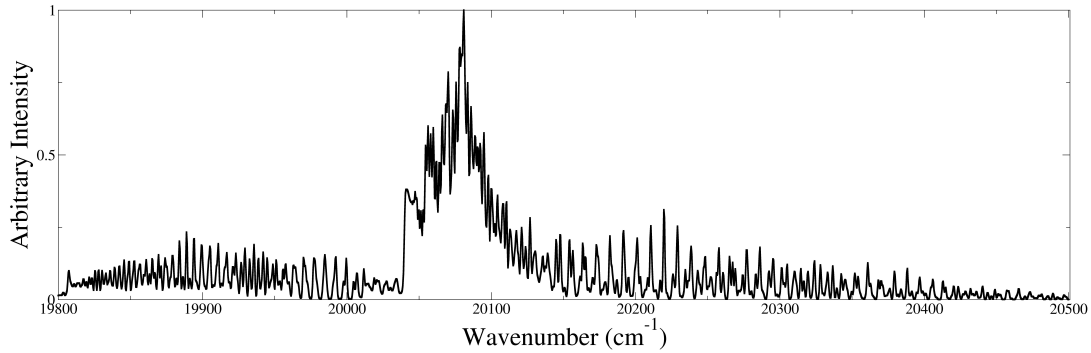

Figure 8. Predicted synthetic spectrum of BeT A – X calculated at $T_{\rm rot}$ = 3800 K and $T_{\rm vib}$ = 4700 K.

expected to be observed in JET during a pure tritium campaign in discharges similar to those in which the BeD spectra were observed. The degree of accuracy in the results for BeT, and any isotopologue of BeH, is expected to be as seen in Figure 6 for BeD. This will be compared with future JET and ITER spectra with their D/T fuel mix.

5. Conclusions

We conclude from a comparison of a synthetic spectrum fitted to experimental BeH and BeD spectra that the PECs, coupling terms, corrective terms and the energies produced by them in Duo are able to accurately reproduce the spectra of BeH, BeD and BeT to good accuracy. The comparisons show discrepancies in the intensities, for example, in the case of the BeD spectrum mostly seen in the Q-branch v = 0 - 0 band head. In the synthetic spectrum, the rotational temperature is too high to match this band head,

which increases in relative intensity with decreasing rotational temperature. There are two possible explanations for this issue: firstly the theoretical model uses a statistical population model, which assumes a thermal equilibrium; the second possibility is that the line of sight for the experimental spectrum passes through different temperature regions, all radiating and giving a cumulative result. The first of these issues will be addressed in a future publication (Darby-Lewis & Tennyson 2018) by introducing a full collisional–radiative population model utilizing vibrationally averaged R-Matrix results from the calculations of Darby-Lewis et al. (2017) extended over bond lengths. The issue with the line of sight can be solved with a line of sight integration calculation applied to the results of the full population model.

Finally in a comparison with the previous work on BeD spectra modelling at JET by Duxbury et al. (1998) we conclude that a better and more comprehensive model has been achieved for two reasons. Firstly, the accuracy of the transition frequency fitting is much increased in our work. Secondly, our model is built using a single dataset derived from all the experimental transition data to model the three isotopologues. Not only does this improve the accuracy of the model, but it also enables accurate predictions to be made for the unobserved BeT isotopologue.

Acknowledgements

We would like to thank Dr. Marie Gorman and Grace Eickmann for sharing their work on MARVEL for BeH, BeD and BeT with us. We would like to thank the Engineering and Physical Sciences Research Council (EPSRC) for studentship (EP/M507970/1) and the Culham Centre for Fusion Energy (CCFE) for funding. This work was carried out within the framework of the EUROfusion Consortium and has received funding from the Euratom research and training programme 2014-2018 under grant agreement No. 633053 and from the RCUK Energy Programme [Grant number EP/P012450/1]. The views and opinions expressed herein do not necessarily reflect those of the European Commssion.

References

Björkas C, Borodin D, Kirschner A, Janev R, Nishijima D, Doerner R & Nordlund K 2013 *Journal of Nuclear Materials* **438**, S276–S279.

Borodin D, Kirschner A, Carpentier-Chouchana S, Pitts R, Lisgo S, Björkas C, Stangeby P, Elder J, Galonska A, Matveev D et al. 2011 *Physica scripta* **2011**(T145), 014008.

Brezinsek S, Stamp M F, Nishijima D, Borodin D, Devaux S, Krieger K, Marsen S, O'Mullane M, Bjoerkas C & Kirschner A a 2014 *Nuclear fusion* **54**, 103001.

Colin R, Dreze C & Steinhauer M 1983 *Can. J. Phys.* **61**, 641–655.

Darby-Lewis D, Masin Z & Tennyson J 2017 *J. Phys. B: At. Mol. Opt. Phys.* **50**, 175201.

Darby-Lewis D & Tennyson J 2018 *J. Phys. B: At. Mol. Opt. Phys.* .

Dattani N S 2015 *J. Mol. Spectrosc.* **311**, 76–83.

De Greef D & Colin R 1974 *J. Mol. Struct. (Theochem)* **53**, 455–465.

Duxbury G, Stamp M F & Summers H P 1998 *Plasma physics and controlled fusion* **40**, 361.

Focsa C, Bernath P F, Mitzner R & Colin R 1998 *J. Mol. Struct. (Theochem)* **192**, 348–358.

Furtenbacher T & Császár A G 2012 *J. Quant. Spectrosc. Radiat. Transf.* **113**, 929–935.

Furtenbacher T, Császár A G & Tennyson J 2007 *J. Mol. Struct. (Theochem)* **245**, 115–125.

Huber K P & Herzberg G 1979 *Molecular Spectra and Molecular Structure IV. Constants of Diatomic Molecules* Van Nostrand Reinhold Company New York.

Koput J 2011 *J. Chem. Phys.* **135**, 244308.

Lasa A, Borodin D, Canik J M, Klepper C C, Groth M, Kirschner A, Airila M, Borodkina I & Ding R 2017 *Nuclear Fusion* .

Le Roy R J, Appadoo D R T, Colin R & Bernath P F 2006 *J. Mol. Struct. (Theochem)* **236**, 178–188.

Le Roy R J, Haugen C C, Tao J & Li H 2011 *Molecular Physics* **109**, 435–446.

Pitarch-Ruiz J, Sanchez-Marin J, Velasco A M & Martin I 2008 *J. Chem. Phys.* **129**, 054310.

Shayesteh A, Tereszchuk K, Bernath P F & Colin R 2003 *J. Chem. Phys.* **118**, 1158–1161.

Tennyson J, Hill C & Yurchenko S N 2013 *in* '6^{th} international conference on atomic and molecular data and their applications ICAMDATA-2012' Vol. 1545 of *AIP Conference Proceedings* AIP, New York pp. 186–195.

Yadin B, Vaness T, Conti P, Hill C, Yurchenko S N & Tennyson J 2012 *Mon. Not. R. Astr. Soc.* **425**, 34–43.

Yurchenko S N, Al-Refaie A F & Tennyson J 2018 *Astron. Astrophys.* . (in press).

Yurchenko S N, Lodi L, Tennyson J & Stolyarov A V 2016 *Computer Phys. Comm.* **202**, 262–275.